Modeling the Formation and the Reduction of Macrosegregation in Continuously Cast Steel Slabs

J. Domitner[1]*, M. Wu[2], F. Mayer[2], A. Ludwig[1,2], B. Kaufmann[3], J. Reiter[4], T. Schaden[5]

[1] Christian Doppler Laboratory for Multiphase Modeling of Metallurgical Processes, University of Leoben, Austria
[2] Chair of Simulation and Modeling of Metallurgical Processes, University of Leoben, Austria
[3] voestalpine Stahl GmbH, Austria
[4] voestalpine Stahl Donawitz GmbH & Co KG, Austria
[5] Siemens VAI Metals Technologies GmbH & Co, Austria
* Franz-Josef-Straße 18, A-8700 Leoben, Austria, e-mail: josef.domitner@unileoben.ac.at

Abstract: In recent years, continuous casting has become the major manufacturing method for semi-finished steel products like slabs, billets or blooms. Many efforts are made to avoid macrosegregation formation near the centreline of these products during solidification. Mainly caused by feeding and bulging induced interdendritic melt flows, positive centreline macrosegregation leads to problems during the succeeding forming processes and to inhomogeneous mechanical product properties. Therefore, the reduction of this unfavourable casting defect brings an essential quality improvement. In continuous strand casting, the mechanical softreduction (MSR) is an effective technology to achieve this. The mechanism of MSR is studied in detail in the current paper. Hence, the macrosegregation formation inside a 25 m long horizontal continuous casting strand was examined for a binary Fe-C-alloy based on an Eulerian-Eulerian multiphase model. Neglecting gravity, the influence of feeding and bulging mechanisms on the formation of macrosegregation inside the strand was investigated. Furthermore, the change of the occurring macrosegregation pattern for a certain MSR configuration was determined.

Key words: steel, continuous casting, softreduction, macrosegregation, multiphase simulation

1. Introduction

Centreline macrosegregation is an undesired casting defect that frequently occurs in the continuous casting process of steel strands. Since this defect can not be removed from the solidified products, controlling the segregation formation immediately during the casting process is crucial to obtain the required steel quality. Industrial practice has shown that the mechanical softreduction (MSR) represents an effective technology to achieve this aim [1-6]. To operate the MSR facilities successfully requires a deep understanding of the macrosegregation formation mechanisms inside the strand. Since experimental plant trials are usually time-consuming and expensive, detailed numerical simulations become increasingly important to understand the phenomenon of macrosegregation formation.

In continuous strand casting, deforming the solid strand shell was identified to cause the formation of positive centreline segregation. Due to the high metallostatic pressure of the liquid melt inside of the strand the thin shell is bulged between adjacent guiding rolls. With advancing solidification the shell thickness increases and therefore this unfavourable effect decreases. First fundamental numerical simulations covering the topic of bulging were conducted by Miyazawa and Schwerdtfeger [7]. Later, the work was extended by Kajitani, Drezet and Rappaz [8] who used a simulation model comprising five roll pairs instead of only a single pair. Nevertheless, compared to industrial continuous casting plant dimensions these models were pretty small. Hence, the authors of the current paper prepared a 2D simulation model according to industrial strand dimensions (total length of 25 m, overall thickness of 285 mm). Based on this model, the influence of bulging on the formation as well as the effect of MSR on the reduction of the centreline macrosegregation was investigated for a binary Fe-C-alloy. To perform the simulations, the commercial software package FLUENT was used.

2. Model description

2.1 Numerical solidification model

To examine the macrosegregation formation inside the strand, a numerical Eulerian two-phase model was utilized [9-11]. It is a simplified version of the three-phase solidification model described in [12-14]. The two considered phases are the liquid melt and the solid columnar dendrites, which grow from the strand's surface towards its centre. Adding up the volume fractions of the solid and the liquid phase, f_S and f_L, results in one. Each of both phases contains two species, iron and carbon.

Since it is difficult to describe the complex morphology of real dendritic structures analytically, the dendrites are assumed to have a cylindrical shape with a constant primary arm spacing λ_1. The solidification is governed by diffusion inside the liquid phase due to a difference between the species concentrations at the cylindrical solid-liquid interface and the species concentrations in the surrounding melt. However, the diffusion inside the solid phase is neglected in the current model. According to the linearized phase diagram for the binary Fe-C-alloy, the thermodynamic behaviour is described by a constant distribution coefficient k and a constant liquidus slope m.

The permeability law required to characterize the hydrodynamic interaction between the liquid melt and the solid dendrites is a modified version of the Blake-Kozeny equation [15]. This equation describes the isotropic permeability K on the entire range of solid fraction f_S. Deep inside the mushy zone at high solid fractions the permeability is quite low and therefore the feeding flow due to solidification shrinkage is completely prevented. Actually, this results in forming local pores or in deforming the already solidified dendrites to compensate the volume change caused by shrinkage. Since both of these mechanisms are not included in the current solidification model, the so called "simplified porosity model" (SPM) is introduced instead. The SPM implies that the density of the solid forming at $f_S > f_S^{SPM}$ deep inside the mushy zone is the same as the density of the melt. Beyond the critical solid fraction f_S^{SPM} no relative motion between the solid dendrites and the remaining interdendritic melt occurs.

To characterize the emerging macrosegregation, the mixture concentration C_M^C is defined for the alloying element carbon, as given in Eq. 1 below. Since the presented solidification model is based on the volume-averaging method, the carbon concentrations C_S^C and C_L^C within both phases, solid and liquid, must be considered to calculate C_M^C.

$$C_M^C = \frac{\rho_S \cdot C_S^C \cdot f_S + \rho_L \cdot C_L^C \cdot f_L}{\rho_S \cdot f_S + \rho_L \cdot f_L} \tag{1}$$

In the current numerical model, the motion of the solid phase is defined analytically according to the surface contour of the casting strand. Therefore, the different 2D strand geometries used in the present simulation study are described in detail hereafter.

2.2 Strand geometry

In this paper, the results of two simulations are compared. Although the performed simulations are based on the same numerical model, two different geometries (G1 and G2) are considered:

- G1: considers bulging
- G2: considers bulging and softreduction

Because both model geometries are similar and G2 can be construed as an extended modification of G1, the further descriptions focus on the more complex geometry G2.

The investigated horizontal continuous casting strand has a total length of l = 25 m and an overall thickness of w = 285 mm. Neglecting the gravity influence on the segregation formation enables to model only one half of the symmetric strand. Therefore the thickness is reduced to $w/2$ = 142.5 mm in the created model. This two-dimensional model geometry representing one half of the continuous casting strand is then subdivided into 4 zones:

- Z1: mould zone
- Z2: bulging zone
- Z3: softreduction zone
- Z4: strand end zone

While the surfaces of Z1 and Z4 are totally flat, those of Z2 and Z3 are sinusoidally waved. The wave troughs indicate the position of the guiding rolls, which are arranged at a constant horizontal distance h. Based on the initial bulging amplitude d_0 at the beginning of Z2, the amplitude decreases linearly towards zero at the end of zone Z3. Additionally, the strand thickness w is continuously reduced within Z3 according to the predefined MSR height s.

To describe the strand surface analytically, the following equations can be applied:

$$y^{surf,Z1} = \frac{w}{2} \tag{2}$$

$$y^{surf,Z2} = \frac{w}{2} - \frac{d_0}{2} \cdot \left(1 - \frac{(x - x_0)}{n \cdot h}\right) \cdot \left(\cos\left(\frac{2\pi \cdot (x - x_0)}{h}\right) - 1\right) \tag{3}$$

$$y^{surf,Z3} = y^{surf,Z2} + \frac{s}{2} \cdot \frac{x - x_1}{x_1 - x_2} \tag{4}$$

$$y^{surf,Z4} = \frac{w - s}{2} \tag{5}$$

In the previous equations, y^{surf} represents the thickness coordinate of the strand surface in the model zones Z1 - Z4, depending on the length coordinate x. All the other symbols occurring in Eq. 2 - Eq. 5 are explained more detailed in Tab. 1.

2.3 Solid phase velocity at the strand surface

The surface velocity of the solid phase in the length direction. $v_{S,x}^{surf}$, is equivalent to the given casting speed v^{cast}. Industrial measurements have shown that the casting velocity does not increase significantly, although the cross section of the strand decreases linearly due to MSR. Therefore,

$$v_{S,x}^{surf,Z1-Z4} = v^{cast}. \tag{6}$$

For each model zone, the surface velocity of the solid phase perpendicular to the casting direction, $v_{S,y}^{surf}$, has to be derived separately from Eq. 2 - Eq. 5:

$$v_{S,y}^{surf,Z1-Z4} = v^{cast} \cdot \frac{\partial y^{surf,Z1-Z4}}{\partial x} \tag{7}$$

According to Eq. 7, $v_{S,y}^{surf}$ = 0 in the zones having a flat surface (Z1 and Z4), while it varies periodically in Z2 and Z3 due to the sinusoidally waved strand surface. In Fig. 1 afterwards, y^{surf}, $v_{S,x}^{surf}$ and $v_{S,y}^{surf}$ are plotted along the entire strand length for all of the 4 model zones. It is obvious that the surfaces of G1 (bulging geometry) and G2 (MSR geometry) only differ in the zones Z3 and Z4.

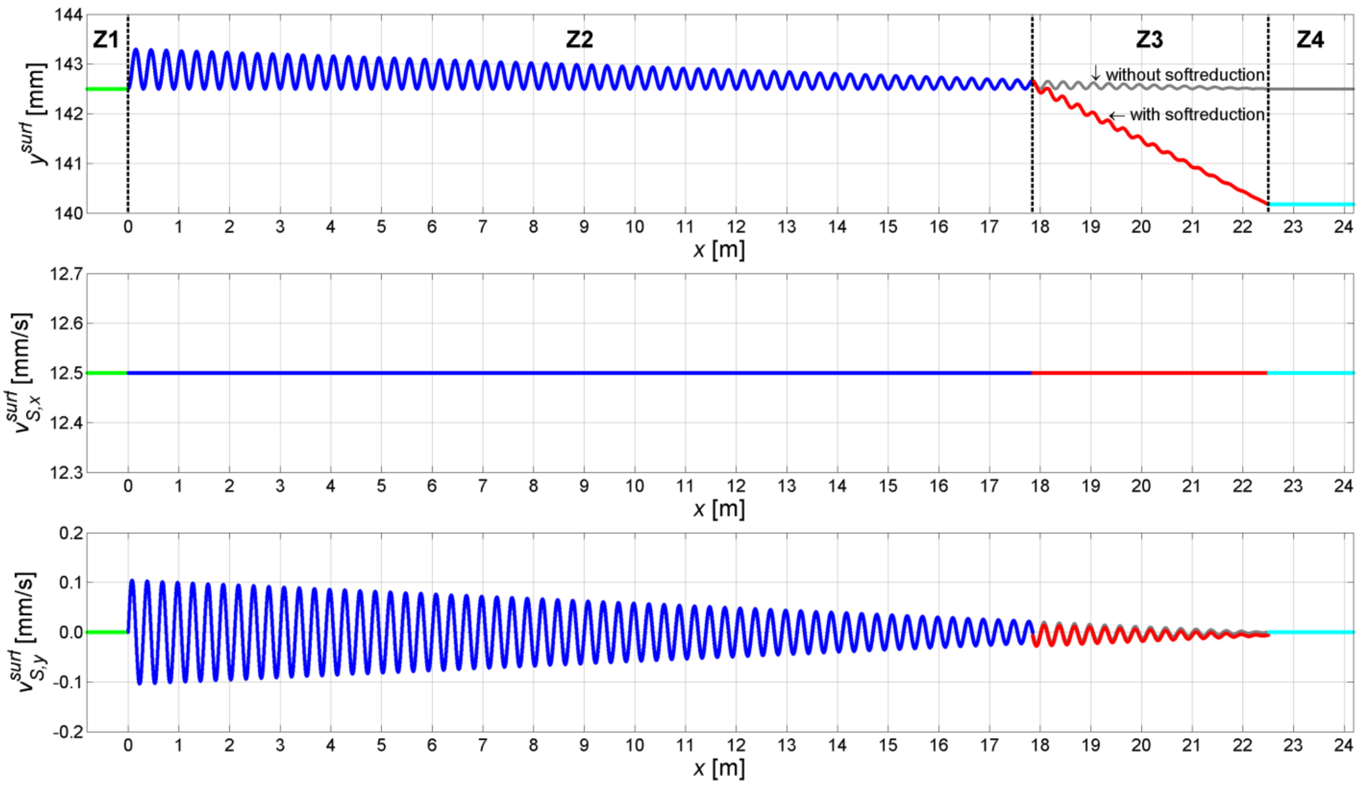

Figure 1: Contour and solid phase velocities in x- and y-direction at the surface of the modeled strand geometries G1 and G2 (green: mould zone Z1, blue: bulging zone Z2, red: softreduction zone Z3, cyan: strand end zone Z4). The grey coloured lines indicate the surface contour of geometry G1 in zone Z3 and zone Z4.

2.4 Inner solid phase velocity

In strand length direction, the inner velocity of the solid phase, $v_{S,x}$, corresponds to the surface velocity $v_{S,x}^{surf}$, which is previously defined in Eq. 6. Hence,

$$v_{S,x}^{Z1-Z4} = v_{S,x}^{surf,Z1-Z4}\,. \tag{8}$$

To prevent undesired relative motion between the liquid and the solid which leads to unphysical macro-segregation formation, the following condition must be fulfilled if $f_S > f_S^{zero}$:

$$\nabla\cdot\left(\rho_S\,\vec{v}_S\right)=0 \tag{9}$$

Rewriting Eq. 9 gives for each of the 4 model zones:

$$\frac{\partial v_{S,y}^{Z1-Z4}}{\partial y} = -\frac{\partial v_{S,x}^{Z1-Z4}}{\partial x} \tag{10}$$

Now, by integrating Eq. 10, the inner velocity of the solid phase perpendicular to the casting direction, $v_{S,y}$, can be obtained:

$$v_{S,y}^{Z1-Z4} = -\int \frac{\partial v_{S,x}^{Z1-Z4}}{\partial x}\,dy \tag{11}$$

Solving the indefinite integral of Eq. 11 separately for each of the model zones Z1 - Z4 delivers an unknown integration constant. For each zone, this constant can be determined by applying the boundary condition $v_{S,y} = v_{S,y}^{surf}$ at $y = y^{surf}$.

The previous definition of the solid velocity component $v_{S,y}$ is appropriate, as long as the dendrites do not meet at the centreline of the strand. However, with advancing solidification the growing dendrites reach the centre and the dendrite tips of both strand halves touch each other. Hence, the touching tips are locally deformed due to the bulging and the MSR movement of the solid. To consider this deformation in the model zones Z2 and Z3 where bulging appears, two sub-domains are distinguished between f_S^{zero} and f_S = 0:

- Domain A ($v_{S,y}^{zero} > 0$): This domain is located behind the guiding rolls. Inside domain A, the dendrites move away from the strand centre. The y-component of the inner solid velocity, $v_{S,y}^{A}$, is equal to the velocity $v_{S,y}^{zero}$ at the solid fraction f_S^{zero}. Therefore,

$$v_{S,y}^{A,Z2-Z3} = v_{S,y}^{zero,Z2-Z3}\,. \tag{12}$$

- Domain B ($v_{S,y}^{zero} < 0$): This domain is located in front of the guiding rolls where the solid is forced to move towards the strand centre. Hence, the previously described deformation of the dendrites between f_S^{zero} and f_S = 0 occurs. Inside domain B, the y-component of the inner solid velocity, $v_{S,y}^{B}$, is assumed to be reduced exponentially from $v_{S,y}^{zero}$:

$$v_{S,y}^{B,Z2-Z3} = v_{S,y}^{zero,Z2-Z3}\cdot\left(1-\exp\left(a\cdot\frac{\left(f_S^{cent}-f_S\right)}{\left(f_S^{zero}-f_S\right)^{b}}\right)\right) \tag{13}$$

The position of the sub-domains A and B inside the model geometry is schematically illustrated in Fig. 2.

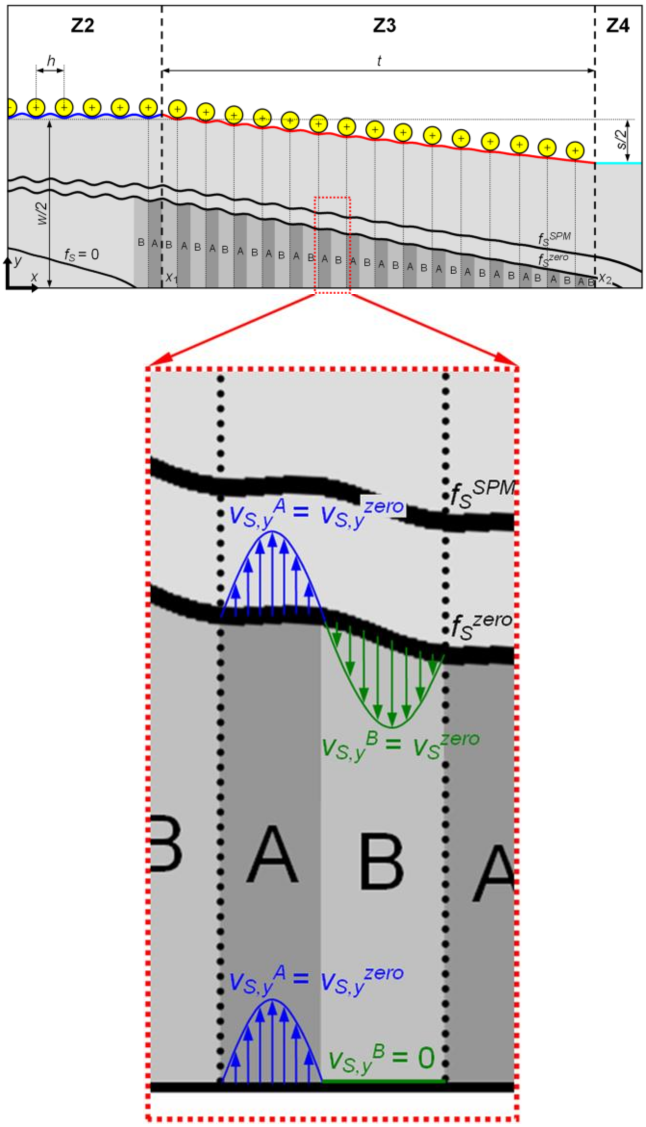

Figure 2: Sub-domains A and B with the corresponding solid phase velocities utilized in the continuous casting model

2.5 Boundary conditions

The environment of the strand is assumed to have a constant temperature T^{envi}. To consider the atmospheric pressure p^{envi} acting on the melt level in the mould, a pressure boundary condition is applied at the inlet of the simulation domain ($x = x_{-1}$). The melt entering the domain through the inlet has the initial carbon concentration $C^{C}_{L,0}$, the initial liquid fraction $f_{L,0}$ and the casting temperature T^{cast}. However, at the outlet of the simulation domain ($x = x_3$), the velocity boundary condition $v_{S,x} = v^{cast}$ is considered. Furthermore, a heat transfer coefficient (HTC) is assigned to those boundaries of the domain, which represent the strand surface. According to industrial investigations, this HTC shows a distinct variation along the strand length. Focussing on the totally horizontal model geometry and neglecting the gravity influence allows using a symmetry condition for the boundary at the strand centre.

Geometrical specifications		
strand length	l	25000 mm
overall strand thickness	w	285 mm
mould length	q	820 mm
initial bulging height	d_0	0.8 mm
distance between guiding rolls	h	300 mm
total number of rolls	n	75
melt meniscus coordinate	x_{-1}	- 820 mm
bulging start coordinate	x_0	0 mm
bulging end coordinate	x_2	22500 mm
strand end coordinate	x_3	24180 mm
Thermophysical data		
density of the liquid phase	ρ_L	7027 kg/m^3
density of the solid phase	ρ_S	7324 kg/m^3
specific heat capacity (liquid)	$c_{p,L}$	808.25 J·kg^{-1}·K^{-1}
specific heat capacity (solid)	$c_{p,S}$	808.25 J·kg^{-1}·K^{-1}
thermal conductivity (liquid)	k_L	29 W·m^{-1}·K^{-1}
thermal conductivity (solid)	k_S	35 W·m^{-1}·K^{-1}
dynamic viscosity (liquid)	η_L	0.0056 kg·m^{-1}·s^{-1}
diffusion coefficient (liquid)	D_L	2·10^{-8} m^2/s
Thermodynamics		
eutectic carbon concentration	$C^{C}_{S,E}$	4.3 wt.%
liquidus slope	m	- 116.7 K/wt.%
distribution coefficient	k	0.36
melting temperature of pure Fe	T^{Fe}_{m}	1811.0 K
latent heat	ΔH_m	2.8·10^5 J/kg
primary dendrite arm spacing	λ_1	1 mm
Boundary conditions		
casting velocity	v^{cast}	0.75 m/min
casting temperature	T^{cast}	1833 K
environment temperature	T^{envi}	309 K
atmospheric pressure	p^{envi}	101325 Pa
initial carbon concentration	$C^{C}_{L,0}$	0.182 wt.%
initial liquid fraction	$f_{L,0}$	0.99999
SPM starting solid fraction	f_S^{SPM}	0.95
zero-strength solid fraction	f_S^{zero}	0.80
empirical constant	a	50
empirical constant	b	0.25

Table 1: Input parameters used in the simulations

3. Results and discussion

3.1 Segregation along the strand thickness

In Fig. 3, the macrosegregation profiles along the thickness direction of the modeled strand are depicted at the coordinate x_3. At this position, the entire cross-section of the strand is solid. Therefore, the segregation shown in Fig. 3 can be found inside the final continuously cast product. Particularly at the strand centre (y = 0), the coloured curves differ distinctly. The green curve representing model geometry G1 indicates positive centreline segregation. In comparison, the blue curve which represents model geometry G2 ends up with negative segregation at the strand centre. To understand the formation of the positive and the negative macrosegregation peaks in detail, the interdendritic flow patterns occurring at the centreline of the strand during solidification are discussed in section 3.3 afterwards.

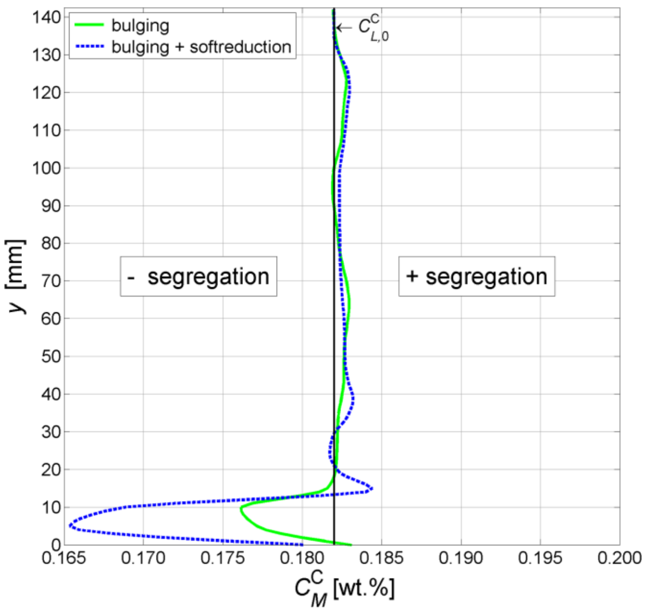

Figure 3: Macrosegregation profiles along the thickness direction of the solidified strand for the model geometries G1 (green curve) and G2 (blue curve)

3.2 Centreline segregation

For both of the simulation geometries, G1 and G2, the obtained macrosegregation and solid fraction profiles along the strand centre are depicted in Fig. 5.

3.2.1 Model geometry G1 (bulging)

On closer examination of geometry G1 (green curve), first macrosegregation appears at x ≈ 16.0 m when the solidification front reaches the centre and the solid fraction starts to rise there. Hence, the segregation formation at the strand centre is related to the appearance of the solid phase. Between x ≈ 16.0 m and x ≈ 21.0 m, the segregation slightly decreases in periodic waves until it reaches a minimum value of C^C_M ≈ 0.179 wt.%. Then the depicted segregation curve changes its direction and increases to the maximum value of C^C_M ≈ 0.183 wt.%. That causes positive segregation at the strand centre which remains inside the cast product after solidification has finished (f_S > 0.95). This typical segregation curve results from the relative motion between the solid and the liquid inside the strand, due to shrinkage feeding and periodic surface bulging. Bulging induces a wavy flow which transports the positive segregated melt towards the strand centre. With increasing number of rolls, the macrosegregation waves sum up. Considering a short academic model geometry, the described behaviour was already ascertained by the current authors [10-11].

At first sight, the positive centreline segregation observed for model geometry G1 seems to be negligibly small. Anyway, it has to be mentioned that the bulging effect on the macrosegregation formation is reinforced, if bulging acts close to the zone of final solidification. Due to the given strand geometry and the chosen boundary conditions this is not achieved in the current simulation study. Herein, the wavy bulging ends and the strand surface becomes flat, although a liquid fraction of f_L ≈ 0.13 still exists at the strand centre. Principally, it is possible to model the situation where bulging acts at the zone of final solidification without changing the previously used geometry G1, just by reducing the predefined casting velocity. As depicted in Fig. 4 below, the segregation maximum increases significantly from C^C_M ≈ 0.183 wt.% (light green curve) to C^C_M ≈ 0.193 wt.% (dark green curve), only by decreasing the casting velocity from v^{cast} = 0.75 m/min to v^{cast} = 0.72 m/min for example.

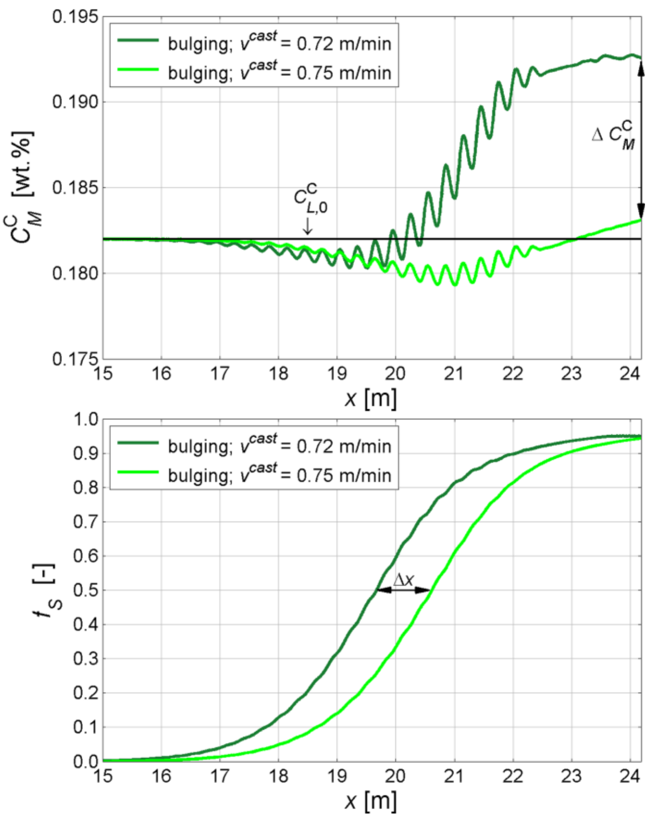

Figure 4: Macrosegregation and solid fraction profiles for two different casting velocities at the strand centre of model geometry G1.

In Fig. 4, the horizontal distance Δx between the almost parallel solid fraction curves indicates the reduction of the metallurgical length due to the lower casting velocity. To achieve a better comparability of the obtained simulation results, the identical casting velocity of v^{cast} = 0.75 m/min was used for both of the model geometries, G1 and G2. Nevertheless, an enhanced simulation study to investigate different casting velocities on the MSR efficiency is in progress.

3.2.2 Model geometry G2 (bulging + MSR)

Hence, to reduce the unfavourable positive centreline segregation, the melt flow caused by bulging inside the strand must be influenced. This can be achieved with MSR, as indicated by the blue curve of Fig. 5. In the present model, MSR starts at a solid fraction of $f_S^{cent} \approx 0.05$ at the centreline. First, reducing the cross section of the strand does not bring the desired improvement on the centreline segregation. Quite the contrary happens, because C_M^C increases rapidly to a positive maximum value of $C_M^C \approx 0.215$ wt.%, which is much higher than the previously observed value without MSR. But then the segregation curve suddenly declines into the range of negative macrosegregation. Finally after solidification has finished, a carbon concentration of $C_M^C \approx 0.180$ wt.% remains at the strand centre. The blue solid fraction curve in Fig. 5 reaches f_S = 0.95 at $x \approx 23.5$ m, while the green curve would reach this solid fraction at $x \approx 24.5$ m. That indicates that MSR reduces the metallurgical length, although the casting velocity is the same for both cases, G1 and G2.

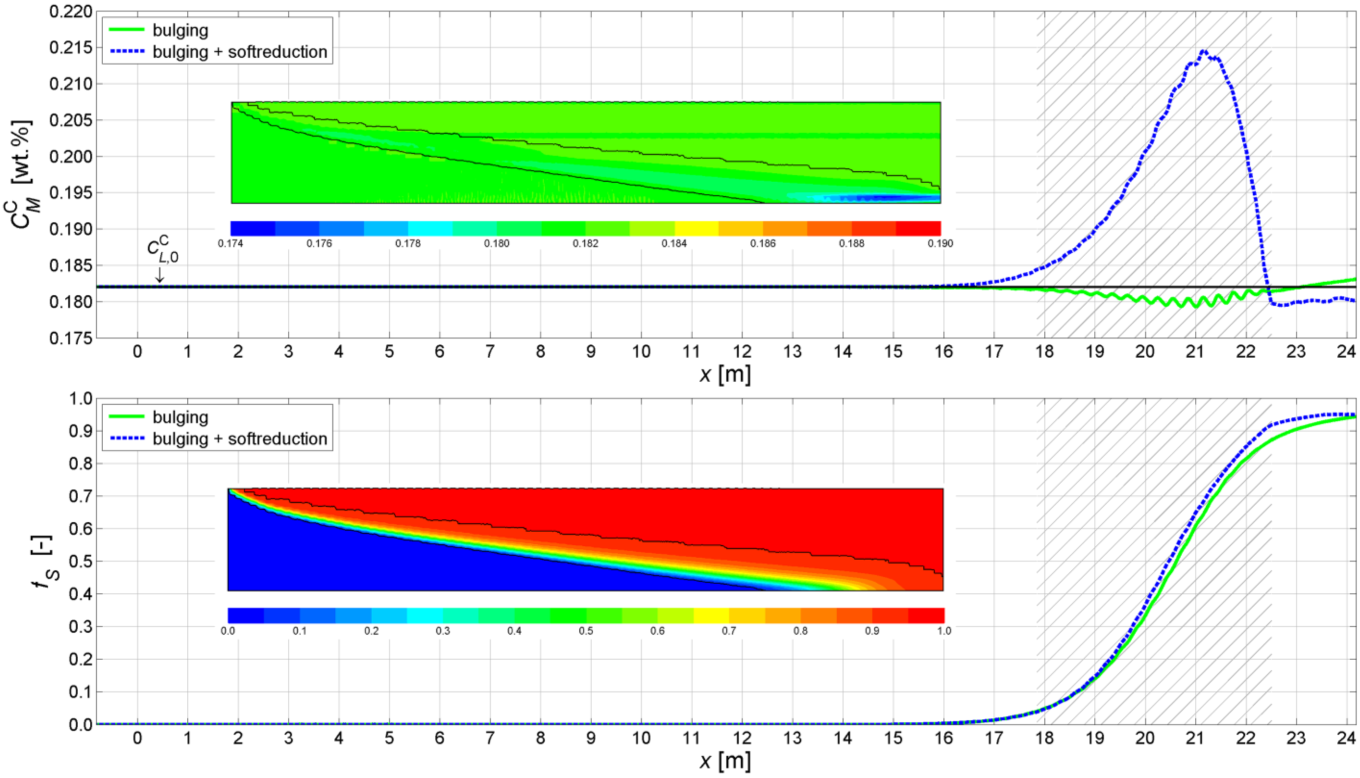

Figure 5: Macrosegregation and solid fraction profiles along the strand centre for the model geometries G1 (green curves) and G2 (blue curves). The hatched areas indicate the position of the MSR zone. For example, the inserted figures in both of the diagrams show the macrosegregation and the solid fraction distribution inside of the simulated strand half (geometry G1, image scaling: x / y = 1/10). The two black curves in each of these figures indicate the mushy zone between the solid fractions of f_S = 0.05 and f_S = 0.95.

3.3 Melt flow patterns

To explain the observed segregation tendency, a detailed examination of the relative melt velocity near the strand centre is advisable. For example, the melt flow patterns at roll 70 (at x = 21.0 m) are compared in Fig. 6 for both of the simulations geometries, G1 and G2. The red arrows indicate the basic melt flow directions inside the mushy zone comprising liquid melt as well as solid dendrites. The mushy zone is delimited by f_S^{SPM}. Beyond this volume fraction solidification has already finished and therefore no relative motion occurs. If only bulging is considered, the highly carbon-enriched melt at the strand centre is pumped in casting direction towards the region of final solidification (Fig. 6a). There, carbon accumulates and positive macrosegregation forms. With increasing solid fraction at the strand centre this pumping effect is reinforced. By contrast, if the strand cross-section decreases due to MSR, the remaining melt at the centre is pressed backwards against the casting direction (Fig. 6b). Since this melt is enriched with carbon, C_M^C between $x \approx 16.0$ m and $x \approx 21.0$ m strongly increases, while it rapidly decreases near the region of final solidification at $x > 21.0$ m.

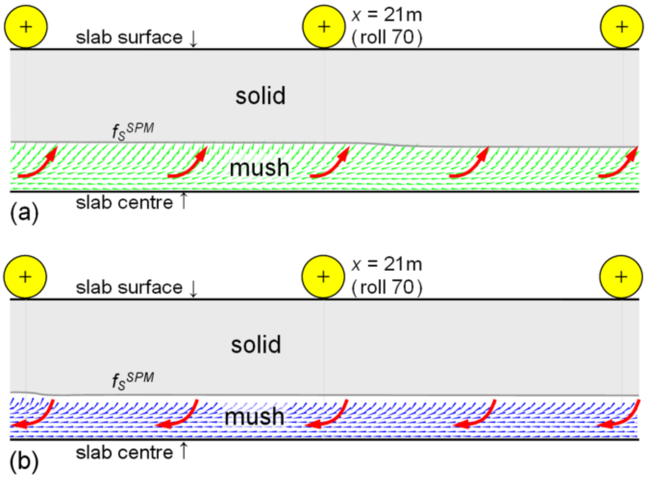

Figure 6: Comparison of the relative velocity patterns inside the mushy zone ("mush") at roll 70 for the geometries G1 (a) and G2 (b). The y - components of the velocity vectors are scaled by a factor of 10.

3.3 Limitations and further improvements

For the numerical simulations presented here, the following remarks should be taken into consideration:

- The current numerical two-phase model describes the macrosegregation formation for a binary Fe-C-alloy. But industrially produced steel grades also contain additional alloying elements (such as Mn, Si, Cr, Mo, ...) which influence the solidification behaviour essentially. In contrast to the simulated binary steel, the metallurgical length and therefore the position of the MSR zone may differ for multi-component steel.
- Since no thermo-mechanical model is implemented, the motion of the solid phase has to be predefined. In sub-domain B, the solid velocity $v_{S,y}^{B}$ is assumed to decrease exponentially towards the strand centre. The exponential approach takes into account, that the main mushy zone deformation occurs close to the centre where the dendrites are quite thin and weak. This assumption is supported by several experimental investigations [16-18]. However, the appropriate determination of the empirical constants a and b required to characterize $v_{S,y}^{B}$ is an open question.
- The presented simulations show, that the interrelation between the position of the bulged surface and the solid fraction appearing at the strand centre has a significant influence on the macrosegregation formation. Since the thermo-mechanical behaviour of the cast material is not considered in the current model, the bulged surface of the continuous casting strand has to be described analytically. Hence, the surface is assumed to be sinusoidally waved. However, although industrial observations confirm this estimation, it is actually unknown how the local bulging height correlates exactly with the solid fraction at the strand centre.
- Since 2D model geometries are used in the present simulations, the width of the continuous casting strand is unconsidered. Therefore, all effects which may concern this direction (e.g. lateral deformation) are not covered. This limitation is of importance for investigating casting formats of small width-to-thickness ratios.
- The numerical model disregards pore and crack formation inside the strand. Especially a deeper understanding of the crack formation could be of interest, because an unfavourable choice of the parameters to operate a MSR device can cause this casting defect. Nevertheless, to study different MSR parameters and their influence on the macrosegregation formation is an ongoing work.

4. Conclusions

In the present paper, the formation of centreline macrosegregation in continuous slab casting is investigated. For that purpose two different 2D model geometries representing a 25 m long strand are compared. One of these geometries considers only the surface deformation of the strand caused by bulging. The other geometry additionally considers the decreasing cross section due to mechanical softreduction (MSR). The performed simulations demonstrate that bulging causes positive centreline segregation, whereas MSR leads to negative centreline segregation inside the totally solidified strand or slab, respectively. At the strand centre, bulging of the solid phase pumps the segregated melt towards the region of final solidification. This interdendritic melt flow pattern inside the mushy zone is significantly modified by MSR. Due to the decreasing cross-section of the strand, the melt enriched with alloying elements is pressed backwards against the casting direction. Therefore, the undesired positive segregation peak is shifted away from the region of final solidification. Instead of this positive peak, a negative segregated region can be found inside the totally solidified continuous casting product.

Acknowledgement

The authors would like to thank the Christian Doppler Research Association (CDG) as well as the industrial partners voestalpine Stahl GmbH, voestalpine Stahl Donawitz GmbH & Co KG and Siemens VAI Metals Technologies GmbH & Co for the financial support of this project.

References

[1] Schwerdtfeger K.: Metallurgie des Stranggießens - Gießen und Erstarren von Stahl; Düsseldorf: Verlag Stahleisen (1992).

[2] Thome R.; Harste K.: Study on the Design of the Soft Reduction Unit of High-Speed Billet Casters; Steel Res. Int., 75 (2004), No. 10, P. 693-700.

[3] Thome R.; Harste K.: Principles of Billet Soft-reduction and Consequences for Continuous Casting; ISIJ Int., Vol. 46 (2006), No. 12, P. 1839-1844.

[4] Preßlinger H.; Ilie S.; Reisinger P.; Schiefermüller A.; Pissenberger A.; Parteder E.; Bernhard C.: Methods for Assessment of Slab Centre Segregation as a Tool to Control Slab Continuous Casting with Soft Reduction; ISIJ Int., Vol. 46 (2006), No. 12, P. 1845-1851.

[5] Bode O.; Schwerdtfeger K.; Geck H. G.; Höfer F.: Influence of casting parameters on void volume and centre segregation in continuously cast 100Cr6 blooms; Ironmak. Steelmak., Vol. 35 (2008), No. 2, P. 137-145.

[6] Ogibayashi S.; Kobayashi M.; Yamada M.; Mukai T.: Influence of Soft Reduction with One-piece Rolls on Center Segregation in Continuously Cast Slabs; ISIJ Int., Vol. 31 (1991), No. 12, P. 1400-1407.

[7] Miyazawa K.; Schwerdtfeger K.: Macrosegregation in continuously cast steel slabs: preliminary theoretical investigation on the effect of steady state bulging; Arch. Eisenhüttenwesen, Vol. 52 (1981), No. 11, P. 415-422.

[8] Kajitani T.; Drezet J.-M.; Rappaz M.: Numerical Simulation of Deformation-Induced Segregation in Continuous Casting of Steel; Metall. Mater. Trans. A, Vol. 32A (2001), P. 1479-1491.

[9] Ludwig A.; Gruber-Pretzler M.; Wu M.; Kuhn A.; Riedle J.: About the Formation of Macrosegregations During Continuous Casting of Sn-Bronze; FDMP, Vol. 1 (2005), No. 4, P. 285-300.

[10] Mayer F.; Wu M.; Ludwig A.: Study of centerline macrosegregation in steel continuous casting with a two-phase volume averaging approach; McWASP XII, TMS Publication (2009), P. 279-286.

[11] Mayer F.; Wu M.; Ludwig A.: On the Formation of Centreline Segregation in Continuous Slab Casting of Steel due to Bulging and/or Feeding; Steel Res. Int., 81 (2010), No. 8, P. 660-667.

[12] Ludwig A.; Wu M.: Modeling the columnar-to-equiaxed transition with a three-phase Eulerian approach; Mater. Sci. Eng. A, Vol. 413-414 (2005), P. 109-114.

[13] Wu M.; Ludwig A.: A Three-Phase Model for Mixed Columnar-Equiaxed Solidification; Metall. Mater. Trans. A, Vol. 37A (2006), P. 1613-1631.

[14] Wu M.; Ludwig A.: Using a Three-Phase Deterministic Model for the Columnar-to-Equiaxed Transition; Metall. Mater. Trans. A, Vol. 38A (2007), P. 1465-1475.

[15] Schneider M. C.; Gu J. P.; Beckermann C.; Boettinger W. J. Kattner U. R.: Modeling of Micro- and Macrosegregation and Freckle Formation in Single-Crystal Nickel-Base Superalloy Directional Solidification; Metall. Mater. Trans. A, Vol. 28A (1997), P. 1517-1531.

[16] Dahle A. K.; StJohn D. H.: Rheological behaviour of the mushy zone and its effect on the formation of casting defects during solidification; Acta Mater., Vol. 47 (1999), P. 31-41.

[17] Shen H. F.; Beckermann C.: An Experimental Study of Deformation of a Columnar Dendritic Mushy Zone Using a Transparent Succinonitrile-Acetone Alloy; Metall. Mater. Trans. B, Vol. 33B (2002), P. 69-78.

[18] Nicolli L. C.; Mo A.; M'Hamdi M.: Modeling of Macrosegregation Caused by Volumetric Deformation in a Coherent Mushy Zone; Metall. Mater. Trans. A, 36A (2005), P. 433-442.